13

Haptic Feedback Modalities for Minimally Invasive Surgery

Min Li[1], Jelizaveta Konstantinova[2] and Kaspar Althoefer[2]

[1]School of Mechanical Engineering, Xi'an Jiaotong University, Xi'an, PR China
[2]School of Mechanical Engineering and Materials Science, Queen Mary University of London ARQ (Advanced Robotics at Queen Mary), London, United Kingdom

Abstract

Sense of touch is critical for surgeons to perform tissue palpation, and there are several tactile sensing that can be used to translate this information (Chapter 5). To overcome the loss of touch, which occurs during robotic-assisted surgical procedures, methods capable of providing partial haptic feedback and mimicking the physical interaction that takes place between surgical tools and human tissue during surgery have been proposed. This chapter introduces haptic feedback modalities for robot-assisted minimally invasive surgical platforms, such as STIFF-FLOP.

13.1 Introduction

During open surgery, which is performed using a single large incision, haptic information can be easily acquired by the surgeons using their hands. In recent years, robot-assisted minimally invasive surgery (RMIS) was widely applied. However, the physical contact between the surgeon and the soft tissue is cut off, which makes acquisition of haptic information during surgeries difficult [1]. Haptic information can be obtained if direct force feedback is provided via a surgical tele-manipulator [2]. However, most current robotic surgical systems, including da Vinci and Titan Medical Amadeus, do not provide haptic feedback.

Alternatively, a graphical display of soft tissue stiffness distribution can be used to show the locations of tumors [3–5]. The benefit of such an approach in comparison to direct force feedback is that it can be applied in combination with complex surgical manipulation when it is undesirable to disturb the performed manipulation. Visualization methods of stiffness distribution the TSS (tactile sensing system) [6–8] and the TIS (tactile imaging system) [9], were developed. However, the visual representation shows only the pressure distribution information within the sensing area. There is no pressure distribution map for the entire organ surface.

Pseudo-haptics is a feedback method attempting to create the illusion of actual haptic feedback through appropriately adapted visual cues without the need for the use of haptic devices [3]. The modification of speed or size of the computer cursor for simulating bumps and holes using a computer mouse and a desktop computer was proposed by previous researchers [4]. A resistance to motion when the cursor approaches an embedded hard nodule in soft tissue during sliding palpation can be simulated by reducing the ratio between the cursor displacement and the computer mouse displacement [5].

Distributed haptics has been introduced for tumor identification in MIS, for instance, the application of tactile sensors and tactile actuators [10]. However, the current application is limited by the complexity and high cost of tactile devices. Multi-fingered haptic feedback conveys more haptic information than single-point force feedback and requires less actuator elements compared to tactile haptic methods.

In this chapter, haptic feedback modalities for minimally invasive surgery are introduced, including force feedback, visual stiffness feedback, pseudo-haptic feedback, and haptic feedback actuators for fingertips.

13.2 Force Feedback

The most common haptic feedback modality is force feedback. Normally, force feedback is provided via a haptic device and conveyed via kinesthetic sensation. In this section we describe the use of force feedback for RMIS. An experimental tele-manipulator and force feedback platform were developed and validated, as part of the STIFF-FLOP project.

13.2.1 Experimental Setup to Validate the Experimental Tele-manipulator and the Force Feedback Platform

The force feedback system consisted of tele-manipulation setup (a slave robot and a master robot) and a vision system. Figure 13.1 displays the schematic

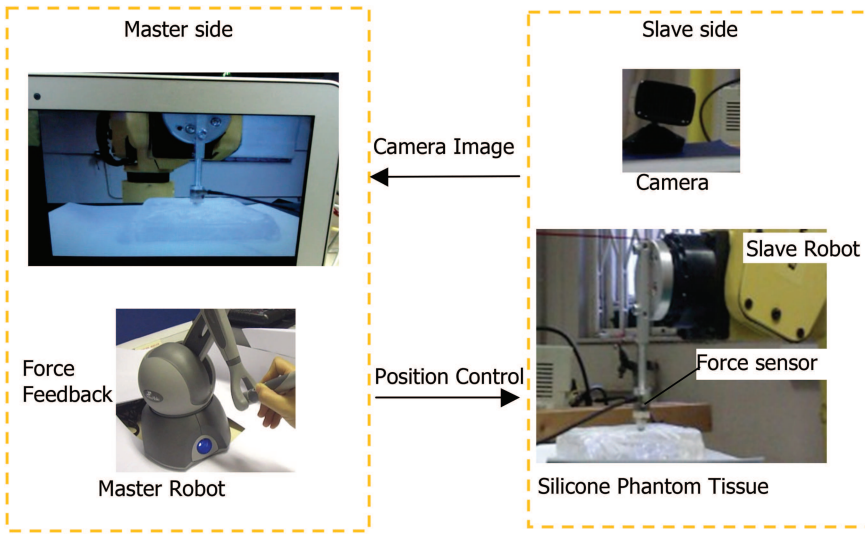

Figure 13.1 Schematic diagram of the haptic manipulator.

diagram of the system design. The right column shows the hardware at the slave side: a camera, a robot arm, a rolling indentation probe [11–13], and a silicone phantom tissue. The left column shows the configuration at the master side: live camera image and force feedback via a haptic device. The middle column lists the software used here. According to the different functions, software was classified into camera image viewer and tele-manipulation. Sensor measurements including force and position were transmitted from the slave side to enable the force feedback on the master side. Real-time images of operational site were also provided using a camera.

A master–slave tele-manipulation configuration was created to simulate the tele-manipulation environment of RMIS. PHANToM Omni (Geomagic Touch) and FANUC robot arm (M-6iB, FANUC Corporation) were used as the master robot and slave robot, respectively, with TCP/IP communication. The main loops of the master and slave sides were synchronized at a frequency of 21.3 Hz. The position of the master robot end-effector was transmitted to the salve side as a control input of the slave robot. The haptic device servo thread ran at a frequency of 1000 Hz. A force sensor was placed at the slave side. FANUC was equipped with an R-J3iC controller with embedded kinematic and dynamic controller. The sequence of the positions provided by the master (PHANToM Omni) was passed directly to the trajectory generator of the robot. In order to avoid discontinuity between the points, the trajectory

generator was set to work in a linear interpolation mode following the hermite curve.

Force measurement used an ATI Nano 17 force sensor (SI-12-0.12, resolution 0.003 N with 16-bit data acquisition card). In order to rapidly scan over a large tissue area [11], a sliding indentation probe [14] was used. In order to reduce the friction during sliding over the tissue, the tissue surface was lubricated with Boots Pharmaceuticals Intrasound Gel. A force distribution matrix can be obtained using the sliding indentation probe, which shows the tissue's Young's modulus at a given indentation depth [15]. It was also found that the indentation speed did not have significant impact on the estimated elastic modulus [15].

Force feedback was applied via a haptic device according to the force sensor measurements at the slave side. The maximum executable force at nominal position of this 3-DOF of force feedback device, PHANToM Omni, was 3.3 N. Force data have three components f_x, f_y, and f_z. The perpendicular reaction force was generated from f_z. The horizontal force was generated from the resultant of f_x and f_y, and the force direction was acquired based on the difference between the previous updated position and the current position (Equation 13.1). The horizontal component vector of the force direction was then transformed to a unit vector with the same direction. The tangent force was provided in the same direction of that tangent unit vector [see Equation (13.2)].

$$V_h \equiv \overrightarrow{P_l P_c}, \tag{13.1}$$

$$\hat{V_h} = \frac{V_h}{|V_h|}, \tag{13.2}$$

where P_l is the previous position (x_l, y_l), P_c is the current position (x_c, y_c), and is the force direction unit vector. If the force value exceeded the maximum output (3.3 N), it was kept at this value.

With the increase in the transparency of the system, jitters generated from small delays and errors in the system often cause unacceptable oscillation of the tele-manipulator. The trade-off between system stability and transparency (matching level of the feedback forces and the forces applied at the tool tip) is a limitation of direct force feedback [16].

In order to validate the proposed experimental tele-manipulator and force feedback platform, a silicone phantom was fabricated (Figure 13.2). The motivation behind this approach is to develop a haptic feedback method that can be used by surgeons during robotic surgery and would assist detection and

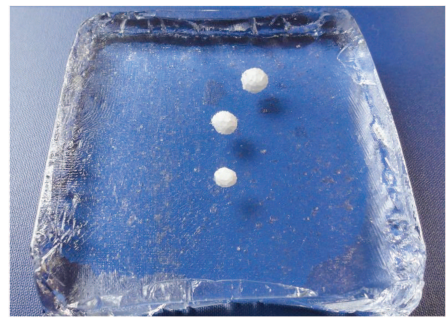

Figure 13.2 Soft tissue silicone phantom with embedded hard nodules to simulate tumors.

localization of stiffer malignant formations. Hard nodules simulating tumors of different sizes were embedded at different depths in the silicone phantom.

13.2.2 Evaluation of the Experimental Tele-manipulator and Force Feedback Platform

Ten human subjects (age range from 23 to 42) were asked to perform a palpation task with tele-operation system using force feedback. All tests were performed by human subjects controlling the slave robot to palpate a silicone phantom tissue with three nodules embedded through the stylus of the PHANToM Omni.

Sensitivity *Se* [17], which represents the test's ability to identify positive results, was defined as:

$$Se = \sum_{i=1}^{n} TP_i \Big/ \sum_{i=1}^{n} (TP_i + FN_i), \tag{13.3}$$

where *TP* is true positives and *FN* is false negatives.

Nodules could be detected using the experimental tele-manipulator and force feedback platform. The nodule detection sensitivity value was 76.7% (95% confidence interval: 59.1–88.2%).

13.3 Visual Stiffness Feedback

Alternative approach to standard haptic feedback methods via kinesthetic sensation is the use of visual modalities. In this section, we describe the use of visual stiffness feedback for RMIS. The benefit of such an approach in comparison to kinesthetic-based methods is that it can be applied in

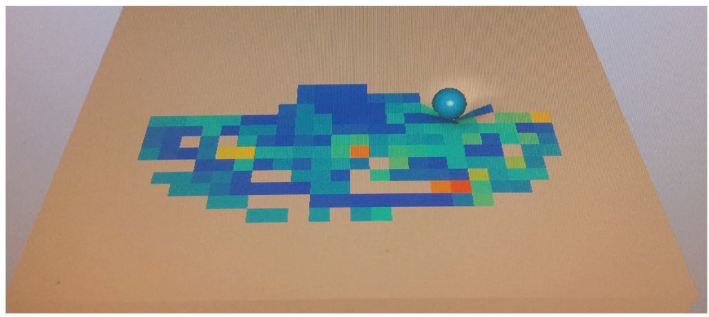

Figure 13.3 Stiffness distribution acquired from the surface of an organ.

combination with complex surgical manipulation when it is undesirable to disturb the performed manipulation. Alternatively, this method can be applied for the use on surgical simulator as a form of assessment. For instance, it is desirable to access the performance of training for a surgeon for a system that is not equipped with force and stiffness measurement devices.

Visual haptic feedback is used to represent the real-time distribution of stiffness acquired from the surface of an organ (Figure 13.3). RGB color-coded map is used to represent the relative stiffness of the tissue, thus, highlighting the areas of high stiffness that are likely to correspond to the location of tumors.

13.3.1 Experimental Setup to Validate the Concept of Visual Stiffness Feedback

To validate the feasibility of visual stiffness feedback, a tele-manipulation setup mimicking the arrangement of surgical robot for minimally invasive surgery was developed (see Figure 13.4). Fanuc robotic arm was used to represent surgical robot with a force sensitive probe for soft tissue palpation. Robotic arm (slave) was controlled by a user using commercially available haptic device (PHANToM Omni). Thus, a trajectory of a robot was defined and controlled by a user via PHANToM Omni device. As in this setting the target was to study visual stiffness feedback only, force feedback option of the haptic device was disabled, and it was used to control the robot position only. Robot trajectory was controlled in a tool coordinate space using position control. Control of a robot was implemented using Ethernet communication. To measure tissue stiffness, a probe with a spherical indenter and force and torque sensor was attached to the end effector of the robot.

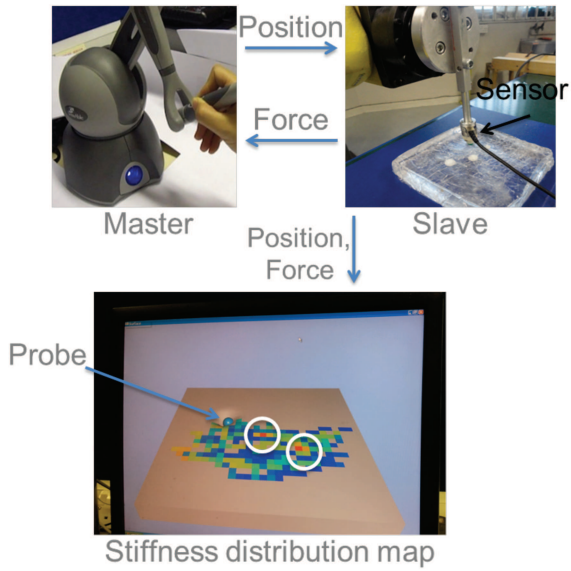

Figure 13.4 Components of tele-manipulation setup: Phantom Omni (master device) is used for position control; Fanuc robot arm (slave device) implements user-defined trajectory; force and torque sensor is embedded in the palpation tool and is used to measure tool and tissue phantom interaction forces; stiffness distribution map displays real-time results of palpation.

In order to validate the proposed approach, the same silicone phantom as described in the previous section was used. The motivation behind this approach is to develop a haptic feedback method that can be used by surgeons during robotic surgery and would assist detection and localization of stiffer malignant formations. The surface of the silicone was modeled on the screen and stiffness distribution was shown after palpation of the certain area. Subject performing remote palpation is facing screen with the simulated organ. Stiffness information was calculated in real time using force magnitude and displacement information of the tool of the robot. The characteristic feature of this algorithm is that the stiffness distribution is displayed as a relative value. An algorithm stores relative minimum and relative maximum values of stiffness. Further on, as soon as a harder region is encountered during palpation, the local maximum value is updated. Harder (stiffer) areas are displayed with higher intensity values of the RGB color map. This approach is feasible for real surgical application, as in most cases, alike during finger palpation, the knowledge about the value of stiffness is not required. More importantly, it is necessary to detect and localize areas of higher stiffness.

The limitation of this method is the need of a tissue model to create realistic stiffness distribution. However, an alternative approach is to employ three-dimensional visual information from endoscopic camera that is typically used together with surgical tools during keyhole surgery.

13.3.2 Evaluation of Visual Stiffness Feedback

Visual stiffness feedback was evaluated during experimental trials with human subjects. Participants were given a task to remotely palpate soft tissue phantom (Figure 13.2) and to explore the surface of a silicone organ using global palpation. Global palpation is a technique used to examine the whole surface of an organ and to define the areas that require thorough examination to determine the presence of abnormalities, such as tumors. This method is very useful to reduce the risk of missing any suspicious regions and can give general information about the state of an organ. As a standard palpation method, it is performed using fingers. In this section, we present the feasibility of the use of global palpation method for tele-manipulated surgery using visual stiffness feedback. There are several ways to perform global palpation technique depending on the type of organ [18, 19].

In the evaluation studies, subjects were first given freedom to apply any desired pattern, and then they were asked to execute the specific pattern of global palpation that is designed to improve palpation performance (Figure 13.7). The second pattern involved scanning of the organ surface from top to bottom using parallel paths, as well as applying circular palpation for the locations where abnormalities are suspected. In addition, circular patterns

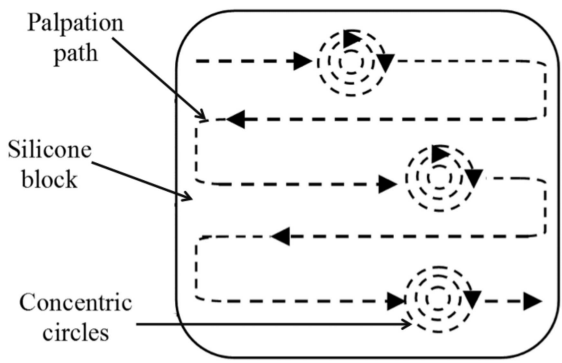

Figure 13.5 Schematic palpation trajectory pattern used to scan the whole surface of the target area with concentric circles applied in the areas of possible inclusions [20].

can give an indication of the stiffness and dimensions of an inclusion in case it is present. Ten subjects were given a task to identify the presence of three simulated abnormalities.

The results of experimental studies shown that subject can reliably use tele-manipulation setup to perform palpation and to identify the presence of hard abnormalities. Average performance of palpation for unrestricted pattern was 73%, while the use of prescribed pattern leads to a higher nodule detection rate with 90% of success. In addition, most subjects indicated that the use of prescribed pattern is easier to apply to detect hard nodules. The involved subjects had little or no palpation experience; however, no difficulties were reported in interpretation of haptic feedback. Therefore, this experiment demonstrates the feasibility of visual stiffness feedback for haptic information in minimally invasive surgery.

13.4 Pseudo-haptic Tissue Stiffness Feedback

Pseudo-haptic feedback combines visual feedback with the resistance of an isometric device [21]. Pseudoforce feedback is generated by changing the pressure on the isometric device [22]. For example, if the user is pressing a spring simulated by an isometric stick, the spring on the screen becomes shorter so that the user has an illusion that the stick is compressed by the user's hand. The stick itself is not compressed. Pseudo-haptic feedback was used to simulate several haptic properties [21], including friction [3], stiffness [3], 22], mass [23], texture [4], and force [24]. In this section, we describe the concept of pseudo-haptic tissue stiffness feedback.

13.4.1 The Concept of Pseudo-haptic Tissue Stiffness Feedback

Pseudo-haptic feedback technique is used to simulate tissue stiffness by changing the ratio of the speed of cursor movement to the speed of finger movement [5, 25]. The user then experiences a corresponding resistance when the cursor speed slows down. Tissue stiffness can also be estimated via visual feedback of the tissue deformation when the applied force is controlled. Visual feedback of tissue surface deformation is required to provide to the user a more realistic feedback of the tissue behavior during palpation. Non-homogeneous stiffness property of soft tissue can be expressed by integrating the sliding behavior simulated by pseudo-haptic feedback with visualization of soft tissue deformation (see Figure 13.6).

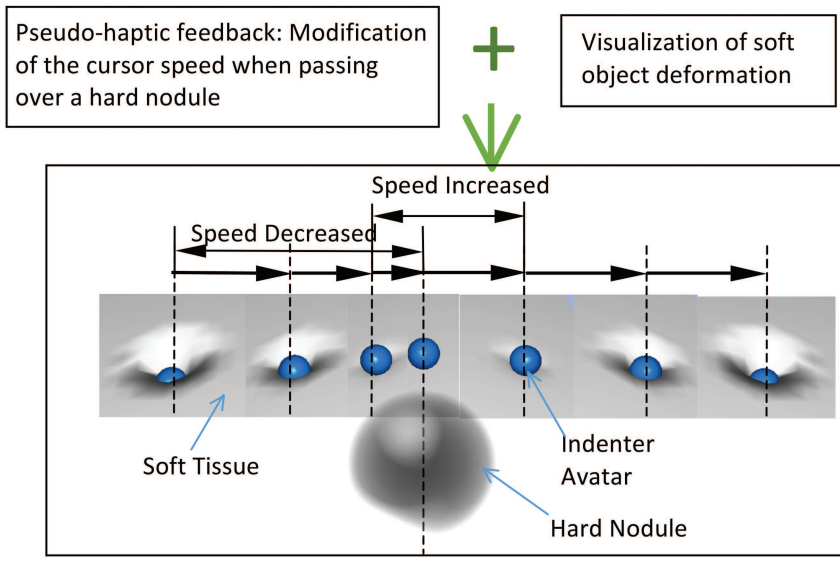

Figure 13.6 Combined pseudo-haptic feedback and visualization of tissue surface deformation [25].

13.4.2 The Combined Pseudo-haptic and Force Feedback

Since the mechanisms of pseudo-haptic feedback and force feedback are fundamentally different, they can be easily combined and will not adversely affect each other [26]. Force feedback was fed to the hand of the user through a haptic device, while the pseudo-haptic feedback information was fed via a graphical interface (see Figure 13.7). The force perception of the user was expected to come from a combination of sensations based on the proprioceptive and visual sensing of the user.

13.4.3 Evaluation of Pseudo-haptic Stiffness Feedback

An experimental validation study aiming at assessing the benefits of the proposed method was performed with the aim to define the efficiency of the proposed methods and to explore the advantages of using a combined pseudo-haptic and force feedback method.

Twenty participants were involved in the experiment: 6 women and 14 men (age range: 23–42). For each test, the same stiffness distribution was used, but the orientation of the silicone block or silicone block model was changed randomly from time to time. During the test, a stopwatch was used

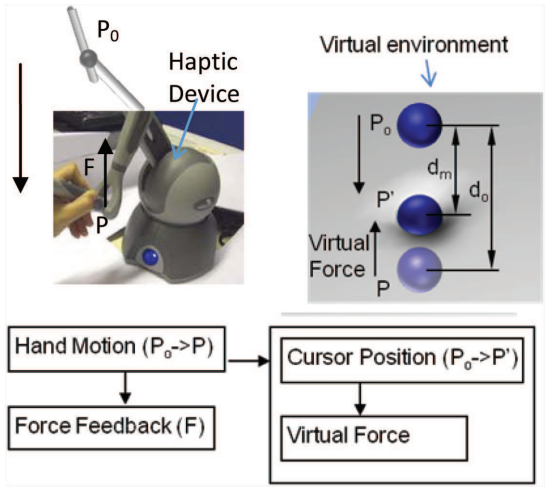

Figure 13.7 Combined pseudo-haptic and force feedback: the left panel is a haptic device, whose stylus is moved from P_o to P, and the right panel is a virtual environment, in which the cursor is supposed to move from P_o to P but actually moved to P′ to create a virtual force.

in order to measure the time required by the participant to detect the hard nodules. The instrument allowed a precision of the time measurement of ± 1 second.

For the test of pseudo-haptic feedback, participants were asked to do a practice run with visible hard nodule locations. Then, they were asked to look for hard nodules in the virtual soft object using pseudo-haptic feedback. The time taken to detect all nodules was recorded. For the test of the combination of pseudo-haptic feedback and force feedback, a practice run of the test was also first conducted. Then, participants were asked to examine the virtual soft object with embedded nodules by using the combined feedback to look for hard nodules. The time needed to detect all nodules was recorded for each participant. These two tests were conducted in a pseudo-random order.

The significance of the difference of sensitivity *Se* between the tests was examined. It was conducted by comparing the observed probabilities (p_1 and p_2) with a combined interval *CI* [27]:

$$CI = \sqrt{(P_1 - P_1)^2 + (P_2 - P_2)^2}, \tag{13.4}$$

where if $p_1 < p_2$, P_1 is the upper bound of p_1 and P_2 is the lower bound of p_2. If $|p_1 - p_2| > CI$, there is a significant difference between the two tests.

Wilson score intervals [28] were calculated at a 95% confidence level.

$$\frac{1}{1+\frac{z^2}{n}}\left[\hat{p}+\frac{z^2}{2n}\pm z\sqrt{\frac{\hat{p}(1-\hat{p})}{n}+\frac{z^2}{4n^2}}\right] \tag{13.5}$$

where $\hat{p}$ is the proportion of successes estimated from the statistical sample; z is the $1-\alpha/2$ percentile of a standard normal distribution; α is the error percentile; and n is the sample size. Here, since the confidence level was 95%, the error α was 5%.

Positive predictive value (*PPV*) [29], which is a measure of the performance of the diagnostic method, was defined as:

$$PPV = \sum_{i=1}^{n} TP \Big/ \sum_{i=1}^{n} (TP + FP)$$

The technique using only pseudo-haptic feedback had a sensitivity *Se* of 50% (37.7–62.3%) overall while the combined technique utilizing both pseudo-haptic feedback and force feedback achieved a sensitivity *Se* of 83.3% with 95% confidential interval 71.9–90.7%. Compared to pseudo-haptic feedback, the *PPV* of the combination method was larger (94% versus 83.3%). Sensitivities *Se* and *PPV* were tested in difference significance. Table 13.1 shows the test results.

As shown in Figure 13.8, the combination method needed less time than the pseudo-haptic feedback test. A Wilcoxon signed-rank test was conducted

Table 13.1 Comparison of nodule detection sensitivities and positive predictive values

	CI	Δp	Significance?
Se	0.167	0.333	Yes
PPV	0.098	0.107	Yes

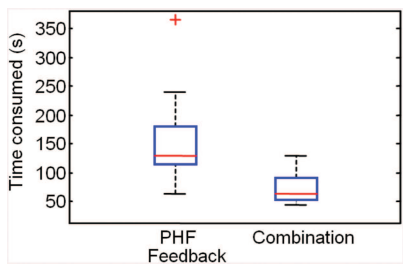

Figure 13.8 Time needed to find nodules using pseudo-haptic feedback and combination technique of pseudo-haptic feedback and force feedback.

Table 13.2 Wilcoxon signed-rank tests for consumed time

n_r	W	$W_{critical}$	Significance
19	4	46	$W < W_{critical}$, Yes

to test the significance of time difference. As shown in Table 13.2, the time difference was significant.

13.5 Haptic Feedback Actuators

Multi-fingered interaction is more common than single-fingered interaction in daily life, and is considered more efficient than single-fingered interaction when conveying haptic information [30]. While multi-fingered haptic feedback conveys more haptic information than single-point force feedback, the actuator elements in a multi-fingered force system can be much reduced compared to tactile haptic methods as, for example, described in [31] and [32]. There are some reports about multi-fingered force feedback for palpation [33–36]. Nevertheless, those devices are relatively expensive. In this section, we describe the use of fingertip haptic feedback actuators for RMIS.

13.5.1 Experimental Setup to Validate the Finger-tip Haptic Feedback Actuators

A pneumatic actuator was used to convey soft tissue stiffness information. Figure 13.10 shows the proposed pneumatic haptic feedback actuator. This actuator is consisted of a deformable surface [including a soft silicone layer (RTV6166 A:B = 1:2, thickness: 3 mm), a silicone rubber membrane (SILEX Ltd., HT6240, thickness: 0.25 mm, tensile strength: 11 N/mm^2, elongation at break: 440%, tear strength: 24 N/mm [37])], a non-deformable PDMS (poly-di-methyl-siloxane) substrate with a cylindrical hole (diameter of 4 mm), air

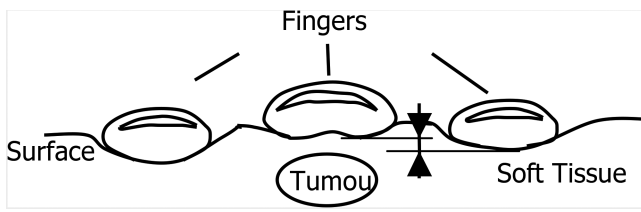

Figure 13.9 Multifinger interaction.

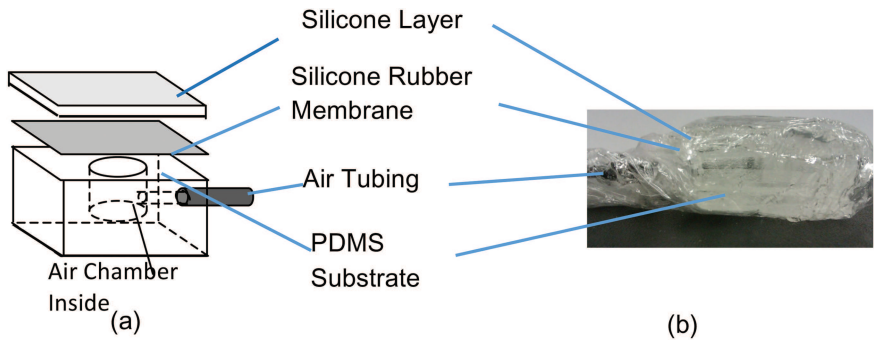

Figure 13.10 A pneumatic haptic feedback actuator: schematic diagram of the components shown in (a) and the prototype shown in (b) [38].

tubing, and a pressure-controllable air supply. When it is in use, air can be injected into the cavity and causes the silicone rubber membrane to inflate. The actuator creates a stress change on the user's fingertip and gives an impression of the stiffness change. The top soft silicone layer was applied to simulate the touch impression of soft tissue and limit the deformation of the silicone rubber film. Translucent silicone rubber adhesive E41 bounded the silicone rubber membrane and the substrate together. The air tubing was connected to the PDMS substrate by using RTV108 clear silicone rubber adhesive sealant. The PDMS substrate was fabricated using 3D prototyped molds.

Figure 13.11 illustrates the control of the proposed pneumatic haptic feedback actuator. The calculation of the three channels of air pressure values relates to the tactile sensing input (e.g., from a tele-manipulator). Data from the tactile sensor elements can be divided into three groups and the average values can be used as the input of a haptic feedback channel. Two NI USB-6211cards were used to generate analog signals for the pressure regulators (ITV0010, SMC). The air compressor (Compact 106, FIAC Air-Compressors) output was set to be 1500 kPa. The pressure regulators decreased the air pressure and inflated each of the actuators with proportional pressures to the analog signals ranging from 0 to 100 kPa. As shown in Figure 13.12, the proposed multi-fingered palpation can be used in RMIS.

To prove the efficiency of the proposed actuator, a user study on palpation using a premeasured stiffness distribution map was conducted. The experimental setup is shown in Figure 13.13. A pressure-sensitive touchpad (Wacom BAMBOO Pen & Touch) was used as an input device of position and normal force. The graphical feedback of the interaction on the tissue

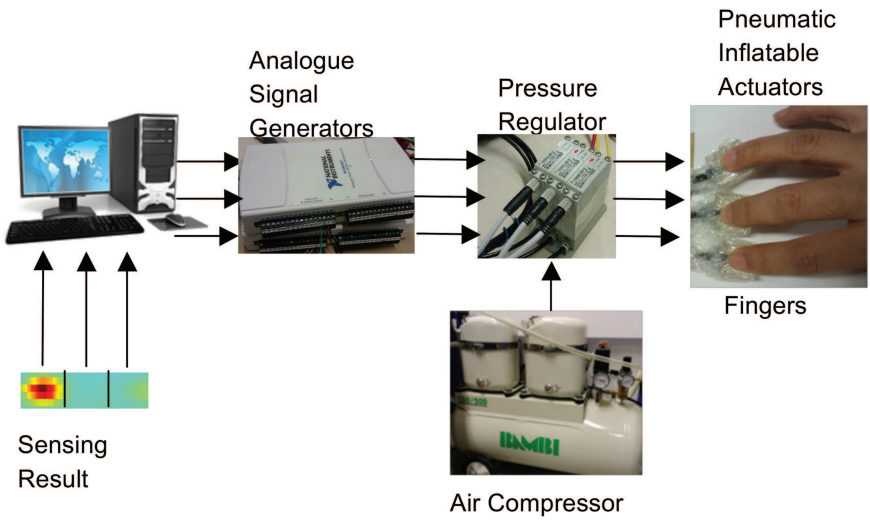

Figure 13.11 Multifingered palpation system [38].

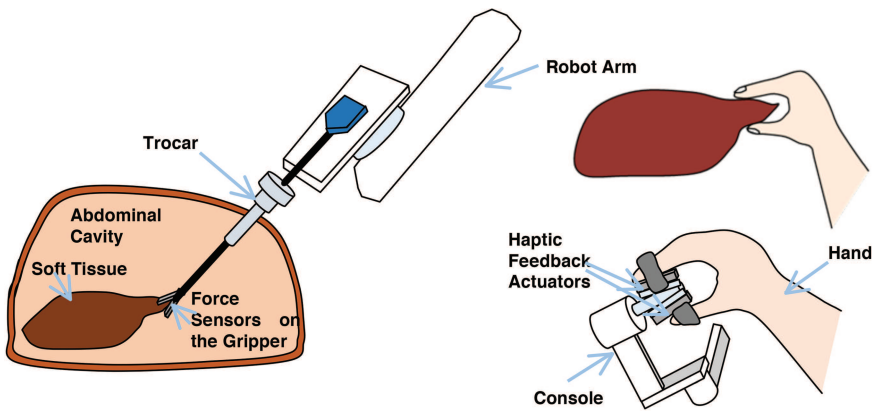

Figure 13.12 Schematic diagram of the applications of the proposed multi-fingered palpation in robot-assisted minimally invasive surgery (RMIS).

surface through computer graphics and the multi-fingered haptic feedback were provided. Three colored spheres displayed on the graphical interface were used to represent three fingers. These three spheres were aligned in a right-angled triangular shape and were set to follow the motion of the pen. The output forces via the pneumatic actuators to the three fingers were translated independently from each other according to the applied palpation

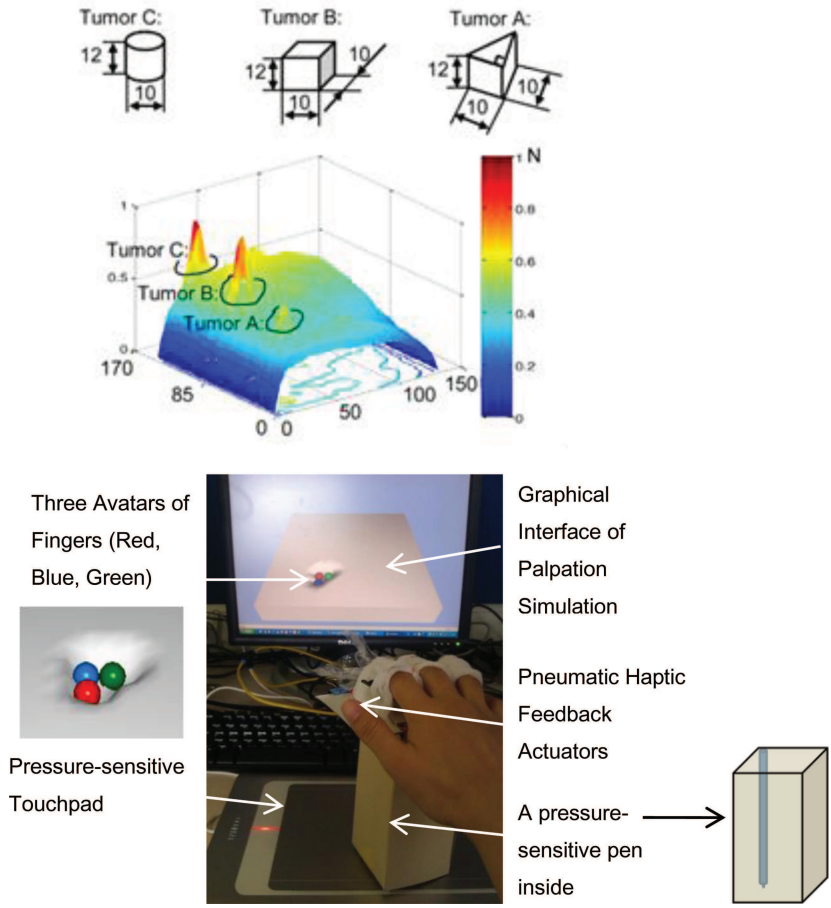

Figure 13.13 Stiffness map and experimental setup for evaluation test [38].

force on the touchpad and the local stiffness value. In this way, users were able to explore three neighboring properties simultaneously.

13.5.2 Evaluation Results of Finger-tip Haptic Feedback Actuators

Nine subjects were involved in this study (age range: 23–36, ♀: 4; ♂: 8). None of them had any palpation experience. In the experiment, all participants could feel the simulated stiffness differences. The measured stiffness distribution came from a silicone phantom soft tissue embedded with artificial

tumors A, B, and C (see Figure 13.13). Tumors were represented as plastic cubes with thicknesses of 4, 12 and 8 mm. The detection sensitivities *Se* of simulated tumor A, B, and C were 66.7, 100, and 88.9%, respectively. There was a positive correlation between the nodule detection sensitivities and nodule sizes.

13.6 Conclusion

In this chapter, haptic feedback modalities for minimally invasive surgery to compensate the loss of physical contact between the surgeon and the soft tissue were introduced and validated, including force feedback from an experimental tele-manipulator and the force feedback platform, visual stiffness feedback representing stiffness distribution of soft tissue, pseudo-haptic feedback expressing haptic perception through a visual display, and finger-tip haptic feedback actuators enabling multi-fingered haptic feedback. Those proposed methods can also be adopted for other applications where sensory substitution is required, including VR-based games and general robotic manipulation.

Acknowledgments

The authors thank the participants of the experiments for their contributions.

References

[1] Gwilliam, J. C., Pezzementi, Z., Jantho, E., Okamura, A. M., and Hsiao, S. (2010).“Human vs. robotic tactile sensing: detecting lumps in soft tissue,” in *Proceedings of the IEEE Haptics Symposium*, 21–28.

[2] Tavakoli, M., Aziminejad, A., Patel, R. V., and Moallem, M. (2006). Methods and mechanisms for contact feedback in a robot-assisted minimally invasive environment. *Surg. Endosc.* 20, 1570–1579.

[3] Lécuyer, A., Coquillart, S., Kheddar, A., Richard, P., and Coiffet, P. (2000). “Pseudo-haptic feedback: can isometric input devices simulate force feedback?,” in *Proceedings of the IEEE Virtual Reality*, New Brunswick, NJ, 83–90.

[4] Lécuyer, A., Burkhardt, J.-M. and Tan, C.-H. (2008). A study of the modification of the speed and size of the cursor for simulating pseudo-haptic bumps and holes. *ACM Trans. Appl. Percept.* 5, 1–21.

[5] Li, M., Liu, H., Li, J., Seneviratne, L. D., and Althoefer, K. (2012). "Tissue stiffness simulation and abnormality localization using pseudo-haptic feedback," in *Proceedings of the IEEE International Conference on Robotics and Automation,* Saint Paul, MN.

[6] Trejos, A. L., Jayender, J., Perri, M. T., Naish, M. D., Patel, R. V., and Malthaner, R. A. (2008). "Experimental evaluation of robot-assisted tactile sensing for minimally invasive surgery," in *Proceedings of the 2nd IEEE RAS EMBS International Conference on Biomedical Robotics and Biomechatronics*, Scottsdale, AZ, 971–976.

[7] Perri M. T., and Trejos, A. L. (2010). New tactile sensing system for minimally invasive surgical tumour localization. *Int. J. Med. Robot. Comput. Assist. Surg.* 6, 211–220.

[8] Perri, M., Trejos, A., and Naish, M. (2010). "Initial evaluation of a tactile/kinesthetic force feedback system for minimally invasive tumor localization," in *Proceedings of theIEEE/ASME Transactions on Mechatronics,* 15, 925–931.

[9] Miller, A. P., Peine, W. J., Son, J. S., and Hammoud, M. D. Z. T. (2007). "Tactile imaging system for localizing lung nodules during video assisted thoracoscopic surgery 1," in *Proceedings of the IEEE International Conference on Robotics and Automation*, Roma, 10–14.

[10] King, C.-H., Culjat, M. O., Franco, M. L., Bisley, J. W., Carman, G. P. Dutson, E. P., et al. (2009). "A multielement tactile feedback system for robot-assisted minimally invasive surgery," in *Proceedings of the IEEE Transactions on Haptics,* 2, 52–56.

[11] Liu, H., Noonan, D. P., Challacombe, B. J., Dasgupta, P., Seneviratne, L. D., and Althoefer, K. (2010). "Rolling mechanical imaging for tissue abnormality localization during minimally invasive surgery," in *Proceedings of the IEEE Transactions on Biomedical Engineering,* 57, 404–414.

[12] Liu, H., Li, J., Poon, Q., Seneviratne, L. D., and Althoefer, K. (2010). "Miniaturized force-indentation depth sensor for tissue abnormality identification during laparoscopic surgery," in *Proceedings of the International Conference on Robotics and Automation (ICRA)*, Anchorage, AK, 3654–3659.

[13] Noonan, D. P., Liu, H., Zweiri, Y. H., Althoefer, K. A., and Seneviratne, L. D. (2007). "A dual-function wheeled probe for tissue viscoelastic property identification during minimally invasive surgery," in *Proceedings of the IEEE International Conference on Robotics and Automation*, Roma, 2629–2634.

[14] Zirjakova, J. (2011). *Prostate Post-surgical 3D Imaging and Data Analysis*. London: King's College.

[15] Liu, H., Li, J., Song, X., Seneviratne, L. D., and Althoefer, K. (2011). Rolling indentation probe for tissue abnormality identification during minimally invasive surgery. *IEEE Trans. Robot.* 27, 450–460.

[16] Okamura, A. M. (2009). Haptic feedback in robot-assisted minimally invasive surgery. *Curr. Opin. Urol.* 19, 102–107.

[17] Altman, D., and Bland, J. (1994). Diagnostic test 1: sensitivity and specificity. *BMJ.* 308:1552.

[18] Wang, N., Gerling, G. J., Childress, R. M., and Martin, M. L. (2010). "Quantifying palpation techniques in relation to performance in a clinical prostate exam," in *Proceedings of the IEEE Transactions on Information Technology in Biomedicine* 14, 1088–1097.

[19] Saunders, K. J., Pilgrim, C. A., and Pennypacker, H. S. (1986). Increased proficiency of search in breast self-examination. *Cancer* 58, 2531–2537.

[20] Konstantinova, J., Li, M., Aminzadeh, V., Althoefer, K., Dasgupta, P., and Nanayakkara, T. (2013). "Evaluating manual palpation trajectory patterns in tele-manipulation for soft tissue examination," in *Proceedings of the IEEE International Conference on Systems, Man, and Cybernetics*, 4190–4195.

[21] Lécuyer, A. (2009). Simulating haptic feedback using vision: a survey of research and applications of pseudo-haptic feedback. *Presence Teleoperators Virtual Environ.* 18, 39–53.

[22] Lécuyer, A. (2001). "Simulating haptic information with haptic illusions in virtual environments," in *Proceedings of the NATO RTA/Human Factors and Medicine Panel Workshop.*

[23] Dominjon, L., Lecuyer, A., Burkhardt, J., Richard, P., and Richir, S. (2005). "Influence of control/display ratio on the perception of mass of manipulated objects in virtual environments," in *Proceedings of the IEEE Virtual Reality*, Bonn, 19–25.

[24] Pusch, A., Martin, O., and Coquillart, S. (2009). HEMP—hand-displacement-based pseudo-haptics: A study of a force field application and a behavioural analysis. *Int. J. Hum. Comput. Stud.* 67, 256–268.

[25] Li, M., Sareh, S., Ridzuan, M., Seneviratne, L. D., Dasgupta, P., Wurdemann, H. A., and Althoefer, K. (2014). "Multi-fingered palpation using pseudo-haptic feedback," in *Proceedings of the The Hamlyn Symposium on Medical Robotics*, London, 3, 8–9.

[26] Hachisu, T., Cirio, G., Marchal, M., and Lécuyer, A. (2011). "Pseudo-haptic feedback augmented with visual and tactile vibrations," in

Proceedings of the IEEE International Symposium on Virtual Reality Innovation, Singapore, 1, 327–328.

[27] Wallis, S. (2013). Binomial confidence intervals and contingency tests: mathematical fundamentals and the evaluation of alternative methods. *J. Quant. Linguist.* 20, 178–208.

[28] Wilson, E. B. (1927). Probable inference, the law of succession, and statistical inference. *J. Am. Stat. Assoc.* 22, 209–212.

[29] Fawcett, T. (2006). An introduction to ROC analysis. *Pattern Recognit. Lett.* 27, 861–874.

[30] Dinsmore, M., Langrana, N., Burdea, G., Ladeji, J., and Box, P. O.(1997). "Virtual Reality Training Simulation for Palpation of Subsurface Tumors," in *Proceedings of the IEEE Virtual Reality Annual International Symposium*, Albuquerque, NM, 54–60.

[31] Kim, S.-Y., Kyung, K.-U., Park, J., and Kwon, D.-S. (2007). Real-time area-based haptic rendering and the augmented tactile display device for a palpation simulator. *Adv. Robot.* 21, 961–981.

[32] Culjat, M., King, C.-H., Franco, M., Bisley, J., Grundfest, W., and Dutson, E. (2008). Pneumatic balloon actuators for tactile feedback in robotic surgery. *Ind. Robot An Int. J.* 35, 449–455.

[33] Langrana, N. A., Burdea, G., Lange, K., Gomez, D., and Deshpande, S. (1994). Dynamic force feedback in a virtual knee palpation. *Artif. Intell. Med.* 6, 321–333.

[34] Daniulaitis, V., and Alhalabi, M. O. (2004). "Medical palpation of deformable tissue using physics-based model for haptic interface robot (HIRO)," in *Proceedings of the 2004 IEEE/RSJ International Conference on Intelligent Robots and Systems,* Sendai, 3907–3911.

[35] Kawasaki, H., Takai, J., Tanaka, Y., Mrad, C., and Mouri, T. (2003). "Control of multi-fingered haptic interface opposite to human hand," in *Proceedings of the 2003 IEEERSJ International Conference on Intelligent Robots and Systems IROS 2003*, Las Vegas, NV, 3, 2707–2712.

[36] Endo, T., Kawasaki, H., Mouri, T., Doi, Y., Yoshida, T., Ishigure, Y., Shimomura, H., Matsumura, M., and Koketsu, K. (2009). "Five-fingered haptic interface robot: HIRO III," in *Proceedings of the World Haptics 2009 Third Joint EuroHaptics conference and Symposium on Haptic Interfaces for Virtual Environment and Teleoperator Systems*, 4, 458–463.

[37] S. S. Ltd. (2014). "*HT 6240 data sheet*."

[38] Li, M., Luo, S., Nanayakkara, T., Seneviratne, L. D., Dasgupta, P., and Althoefer, K. (2014). Multi-fingered haptic palpation using pneumatic feedback actuators. *Sensors Actuators A Phys.* 218, 132–141.

[39] Yamamoto, T., and Abolhassani, N. (2012). Augmented reality and haptic interfaces for robot-assisted surgery. *Int. J. Med. Robot. Comput. Assist. Surg.* 8, 45–56.